JACS
JOURNAL OF THE AMERICAN CHEMICAL SOCIETY
pubs.acs.org/JACS
Article

Achieving Efficient Organic Room-Temperature Phosphorescence through Acceptor Dendronization

Chensen Li,‡ Zhenchen Lou,‡ Minghui Wu,‡ Fulong Ma,‡ Xinmeng Chen, Haozhe Tan, Zonghang Liu, Feng Gao, Zijie Qiu, Zheng Zhao,* Lianrui Hu,* Guohua Xie,* Maoqiu Li, Yumeng Guo, Zhongjie Ren,* Song Zhang, Yuchao Liu, Shouke Yan, Zhen Li, Bo Xu, Ryan T. K. Kwok, Jacky W. Y. Lam, and Ben Zhong Tang*

Cite This: J. Am. Chem. Soc. 2025, 147, 18317−18326
Read Online
ACCESS | Metrics & More | Article Recommendations | Supporting Information

ABSTRACT: Organic room-temperature phosphorescence (RTP) materials hold significant promise for applications in optoelectronics, information security, and bioimaging. Recently, significant progress has been made in RTP materials and vacuum-deposited organic light-emitting diode (OLED) devices. However, the performance of solution-processed OLEDs is seriously lagging behind due to the lack of RTP molecular strategies that balance exciton stability and solution processability at the single-molecule scale. In this work, we propose an acceptor dendronization strategy for designing RTP materials and successfully achieving highly efficient and stable RTP emissions. This strategy can simultaneously enhance the various processes involved in RTP emission at the single-molecule level: increase the intersystem crossing channels, enhance the spin−orbit coupling constants between T_1 and S_0, and suppress molecular motion. Consequently, it promotes intersystem crossing and triplet radiative transition while inhibiting nonradiative transition, thereby efficiently enhancing RTP emission. A proof-of-concept acceptor-dendronized dendrimer exhibits long phosphorescence lifetimes in the millisecond range in ambient solution and near 100% photoluminescent quantum yields in the doped films. This is the first reported RTP dendrimer to date. An OLED fabricated using this dendrimer in a sky-blue emission achieves an external quantum efficiency of 25.1%, which represents the state-of-the-art efficiency based on solution-processed RTP-OLEDs to date. Our findings offer definitive guidelines for the molecular engineering of RTP materials and pave the way for innovative RTP systems in diverse optoelectronic applications.

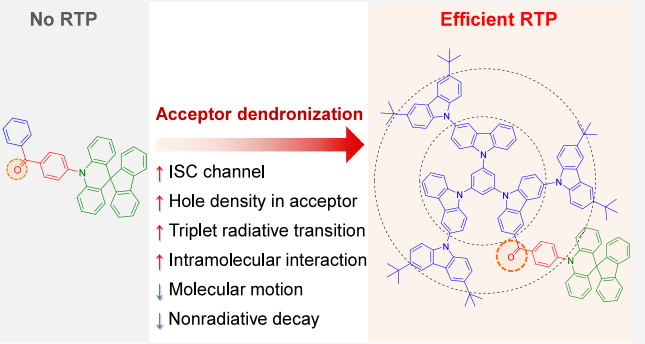

INTRODUCTION

Organic room-temperature phosphorescence (RTP)[1−5] has emerged as an attractive research topic with multiple potential applications in optoelectronic devices,[6] information anticounterfeiting,[7] biomedical imaging,[8] phosphorescence probes,[9] and biosensing.[10] This interest is due to the full utilization of the radiative relaxation of the triplet excited state. Although numerous RTP materials have been developed, their inefficient phosphorescence at room temperature is the main limitation for practical applications. The primary challenges include two aspects: First, the spin forbidden property leads to insufficient intersystem crossing (ISC),[11] and the intrinsic phosphorescence quantum yield is generally lower than the theoretical limit. Second, traditional methods such as crystallization,[12,13] matrix rigidification,[14,15] and supramolecular self-assembly[16,17] rely on constructing rigid confinement environments to enhance exciton stability, but these approaches sacrifice material processability, making it difficult to meet practical applications. In recent years, researchers have been trying to develop different strategies to improve the RTP efficiency, including vacuum evaporation and solution processing-type RTP materials. The main strategies include: introducing heteroatoms (O, N, S, and P)[4] with abundant lone pair electrons to enhance spin orbit coupling (SOC), building twist donor−acceptor (D-A) structures to reduce the single triplet energy gap difference (ΔE_{ST}),[18] and constructing rigid confinements to suppress molecular motion to reduce nonradiative transitions[19] (Figure 1). For example, Su et al.[20] reported a phenoxyselenide donor-triazine acceptor molecule exhibiting a strong SOC (S_0, T_1) of 108.48 cm^{-1} and multiple hydrogen bonds that rigidify the molecular skeleton. The corresponding vacuum deposited organic light-emitting diode

Received: April 14, 2025
Revised: May 7, 2025
Accepted: May 7, 2025
Published: May 16, 2025

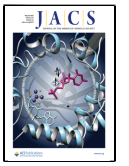

https://doi.org/10.1021/jacs.5c06288
J. Am. Chem. Soc. 2025, 147, 18317−18326

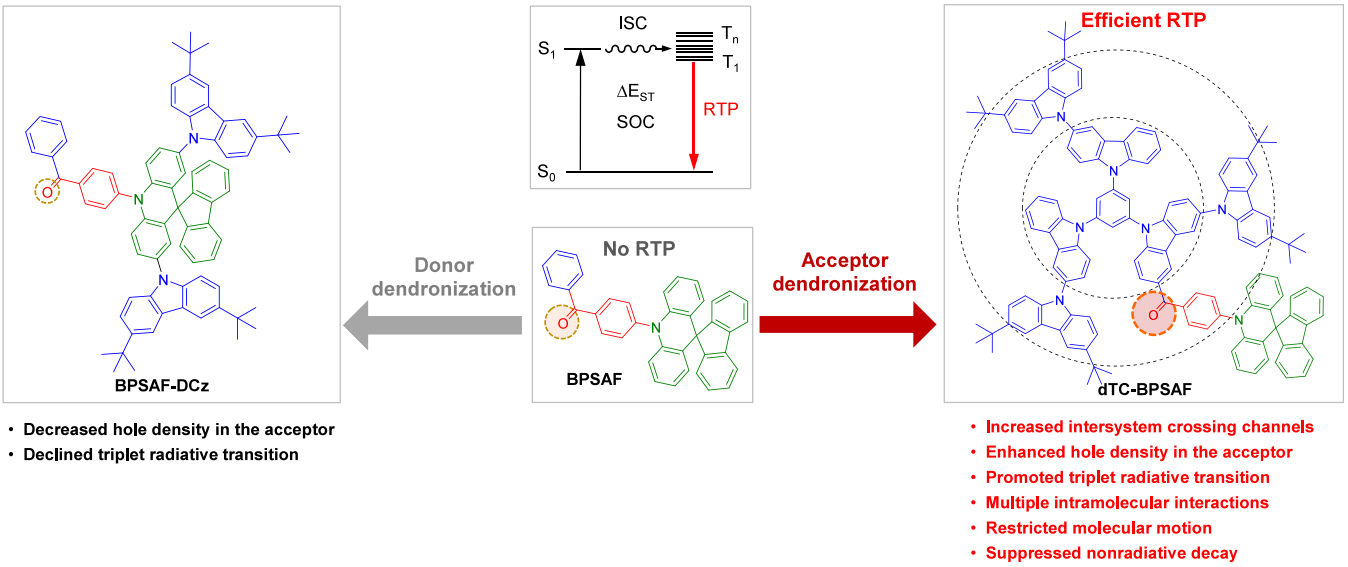

Figure 1. Schematic diagram of the luminescence mechanism of efficient room-temperature phosphorescence (RTP) achieved through acceptor dendronization and the chemical structure of small molecular BPSAF, donor-dendronized BPSAF-DCz, and acceptor-dendronized dTC-BPSAF. ΔE_{ST}: energy gap between singlet and triplet states; SOC: spin−orbit coupling; ISC: intersystem crossing.

(OLED) device achieved an external quantum efficiency (EQE) of 19.5%. Additionally, Zhao et al.[21] demonstrated a rigid indolocarbazole-xanthenone system with a ∼60° twist angle, achieving a small ΔE_{ST} (0.28 eV) and a high PLQY (72%), leading to a nondoped vacuum-deposited OLED with a record EQE of 24.9%.

In comparison, solution-processed OLEDs[22] offer advantages such as low-cost fabrication, high material utilization, simple processing (e.g., inkjet printing or spin coating), and compatibility with flexible/large-area devices. Early molecular designs focused on enhancing SOC through heteroatoms/heavy atoms. For example, Ceroni et al.[23] reported a thiophenol-functionalized benzene derivative with six flexible substituents, but excessive molecular motion limited its device EQE to only 0.1%. Later, Ding et al.[24] developed an oxygen-containing D-A-structured RTP polymer, where oxygen atoms reduced orbital overlap to enhance SOC while polymer rigidity suppressed nonradiative decay. This system achieved a solution-processed OLED EQE of 9.7%. However, solution-processed RTP devices currently show significantly lower efficiencies than vacuum-deposited counterparts (EQE < 10% vs >20%). The bottleneck stems from conflicting requirements: solution processability necessitates flexible molecular designs, whereas suppressing nonradiative triplet deactivation demands rigid environments.

Dendrimers[25−28] hold potential to construct efficient solution-processed RTP materials owing to their unique advantages, including abundant functional adjustability, high morphological stability, and excellent solution processability. These properties may overcome the efficiency bottleneck of solution-processed RTP-OLED devices. However, research on RTP dendrimers remains rare due to the absence of established molecular design principles. The conventional donor-dendronization strategy—introducing dendrons into donors to form acceptor−donor−dendron (A-D-D′) architectures—has failed to exhibit RTP. This approach excessively strengthens electron-donating effects, depletes hole density in the acceptor's triplet state, and consequently weakens spin−orbit coupling (SOC) while impeding efficient spin-flip processes. A promising alternative involves increasing the acceptor's triplet hole density through acceptor dendronization. For instance, the thermally activated delayed fluorescence (TADF)[29,30] molecule BPSAF[31] (Figure 1) combines a strong carbonyl acceptor with a spiro[acridine-9,9′-fluorene] (SAF) donor, achieving both a small ΔE_{ST} and a large SOC constant. Nevertheless, despite efficient ISC in BPSAF and other TADF systems, RTP emission remains elusive. Highly branched dendrimers, such as 1,3,5-tris(3′,6′-di-*tert*-butyl-9*H*-[3,9′-bicarbazol]-9-yl)benzene (TC), contain rigid and bulky peripheral carbazole dendrons. When these dendrons are attached to a benzophenone (BP) acceptor to form a donor−acceptor−dendron (D-A-D′)-typed asymmetric dendrimer (dTC-BPSAF) (Figure 1), they not only increase intramolecular interactions, which lead to energy level splitting and an enhancement of ISC channels, but also enhance the hole density of triplet and $^3(n, \pi^*)$ characteristics in the BP acceptor, resulting in high SOC constants for efficient triplet radiation.

In addition, the dTC-BPSAF dendrimer also demonstrates multiple molecular interactions and a rigid dendronized structure, which lead to restricted molecular motion, stabilized triplet excitons, and suppressed nonradiative transitions, thereby resulting in efficient RTP emission in solution. Experiments conducted with the dendrimer in ambient dilute toluene solution demonstrate that despite the presence of dissolved oxygen at a concentration of 8.67×10^{-3} M[32] at room temperature, the RTP emission remains ultrastable in both aerated and deaerated solutions. These results indicate that the dendrons attached to the acceptor can also effectively protect the triplet excitons of dTC-BPSAF from being quenched by oxygen, thereby achieving ultrastable RTP emission in ambient solution with a photoluminescence quantum yield (PLQY) of 34%. Furthermore, to further reduce molecular motion and quenching of triplet excitons, the dTC-BPSAF dendrimer was doped into the host films, resulting in a high PLQY of ∼100%. Additionally, the solution-processed RTP-OLEDs achieved a record-high EQE of 25.1%. These remarkable results validate the effectiveness of

https://doi.org/10.1021/jacs.5c06288
J. Am. Chem. Soc. 2025, 147, 18317−18326

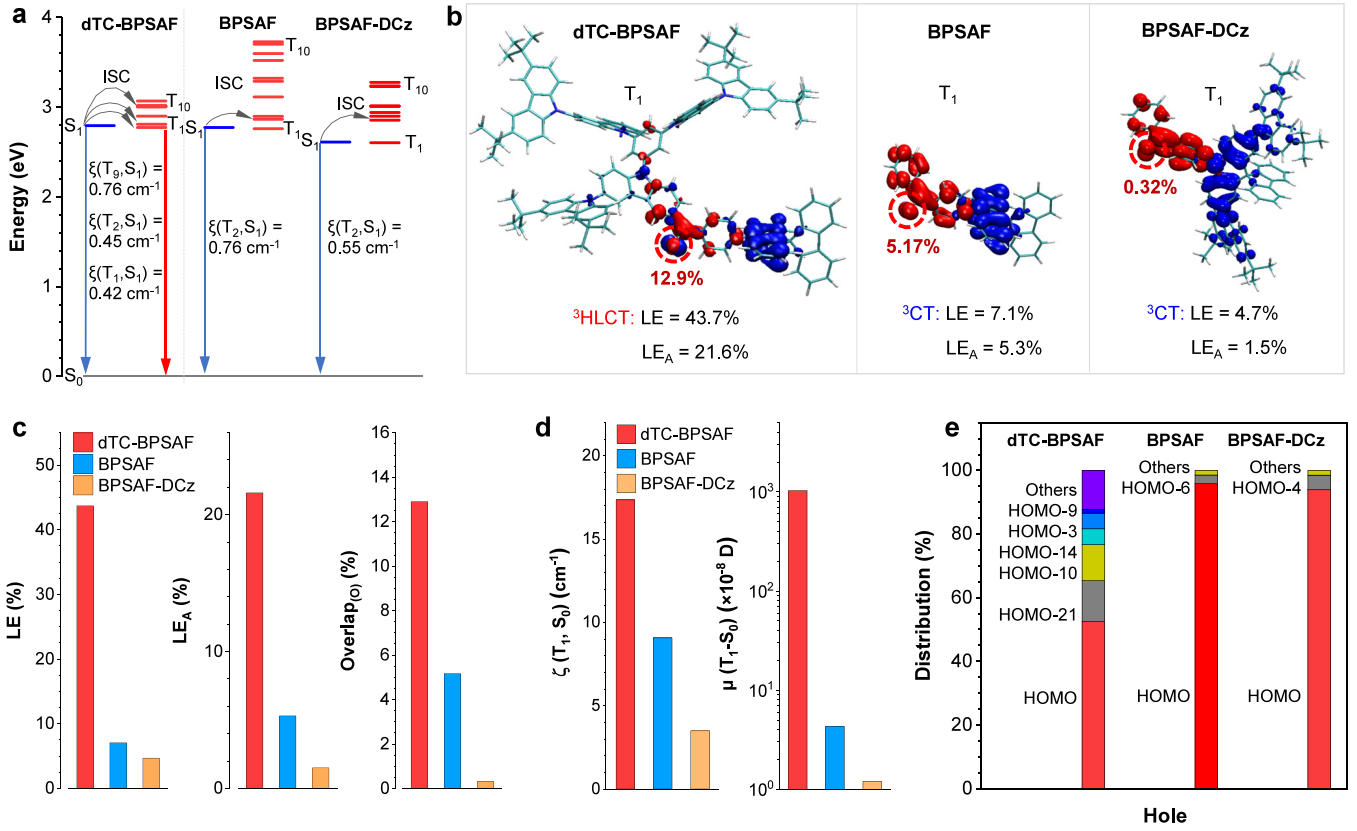

Figure 2. Quantum chemical calculations of the excited-state properties of dTC-BPSAF, BPSAF, and BPSAF-DCz. (a) The excited states, intersystem crossing (ISC) processes, and spin−orbit coupling (SOC) constants (ξ) of dTC-BPSAF, BPSAF, and BPSAF-DCz. (b) The distributions of hole (blue colored) and electron (red colored) in the T_1 state of dTC-BPSAF, BPSAF, and BPSAF-DCz. (c) The proportion of the locally excited (LE) state (left), the LE proportions of BP acceptor (middle), and the hole−electron overlap of the carbonyl oxygen (right) in the T_1 state of dTC-BPSAF, BPSAF, and BPSAF-DCz. (d) The SOC constants (ξ) and transition dipole moments (μ) for the radiative T_1−S_0 transition of dTC-BPSAF, BPSAF, and BPSAF-DCz. (e) The contributions of HOMOs to the hole in the T_1 state of dTC-BPSAF, BPSAF, and BPSAF-DCz.

the acceptor dendronization strategy for achieving efficient RTP both in solution and in solid states, elucidating the mechanism of restricting molecular motion to achieve efficient RTP.

RESULTS AND DISCUSSION

Quantum-Chemical Calculations. The acceptor dendronization strategy can effectively regulate the population of triplet excitons by increasing the splitting of triplet energy levels and enhancing the proportion of locally excited (LE) characteristics of the acceptor in the lowest triplet state (T_1) state. These two factors are anticipated to promote ISC processes from the lowest singlet (S_1) to T_1 and triplet radiative transitions from the T_1 back to the ground state (S_0), thus achieving highly efficient RTP. To analyze and predict the feasibility and reliability of the acceptor-dendronized strategy, quantum-chemical calculations were performed on dTC-BPSAF, BPSAF, and the donor-dendronized dendrimer BPSAF-DCz for comparison, to investigate two crucial photophysical processes: (1) the enhancement of ISC spin-flipping processes from the S_1 to triplet state (T_n) (k_{ISC}) and (2) the facilitation of the phosphorescent decay rate from the T_1 to the S_0 (k_p). The ISC process was evaluated based on eq 1.[33]

$$k_{ISC} \propto \sum_n |\langle S_1|\hat{H}_{SOC}|T_n\rangle|^2 \exp(-E^2_{S_1T_n}) \quad (1)$$

where a smaller ΔE_{ST}, coupled with more ISC channels and larger spin−orbit coupling operator ($\hat{H}_{SOC}$), can enhance k_{ISC}. First, dTC-BPSAF inherits the HOMO and LUMO distributions of BPSAF (Figure S1), resulting in a very small ΔE_{S1-T1} (0.02 eV). Second, the introduction of dendrons increases the density of triplet states and reduces the triplet−triplet energy gaps (ΔE_{TT}), which increases valid ISC channels ($\Delta E_{ST} \leq 0.3$ eV and SOC ≥ 0.3 cm^{-1}) from S_1 to T_n.[34] Specifically, the number of valid ISC channels of dTC-BPSAF is three ($S_1 \rightarrow T_1$, T_2, and T_9) (Figure 2a), while the ISC channels of BPSAF is only one ($S_1 \rightarrow T_2$ with a ΔE_{S1-T2} of −0.09 eV). In comparison, donor-dendronized BPSAF-DCz also exhibits only one ISC channel ($S_1 \rightarrow T_2$) with a ΔE_{S1-T2} of −0.24 eV. Although donor dendronization increases the density of triplet states, it fails to enhance the effective ISC channels. These results indicate that acceptor dendronization is an effective strategy to enhance the ISC process by increasing the number of ISC channels.

Additionally, the large SOC (T_1, S_0) and the transition dipole moment between the T_1 and S_0 states ($\mu_{T_1 \rightarrow S_0}$) are also significant factors in achieving efficient RTP, and the wave function properties[35,36] of T_1 are crucial elements affecting SOC (T_1, S_0) and $\mu_{T_1 \rightarrow S_0}$. Figure 2b illustrates the distribution of holes and electrons in T_1 for the three compounds. In dTC-BPSAF, electrons are predominantly localized on the BP acceptor (83.0%), while holes are mainly localized on the SAF donor (57.9%), with a partial localization on the BP acceptor

https://doi.org/10.1021/jacs.5c06288
J. Am. Chem. Soc. 2025, 147, 18317−18326

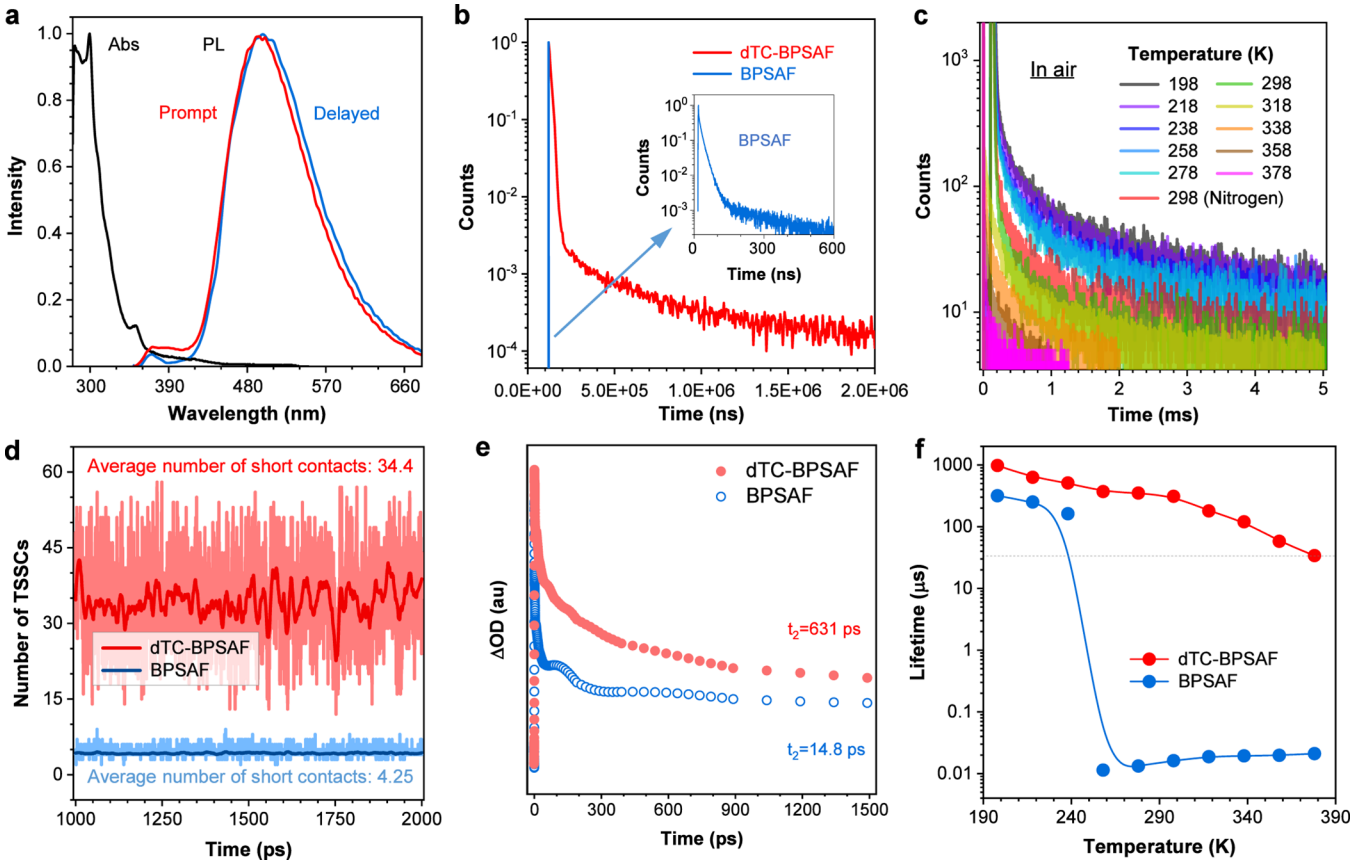

Figure 3. Photoluminescence (PL) behaviors and intramolecular interactions of dTC-BPSAF and BPSAF. (a) The absorption (Abs) spectrum and the prompt and delayed PL spectra of dTC-BPSAF in toluene (10 μM) at room temperature; excitation wavelength (λ_{ex}) = 330 nm. (b) The transient PL decay curves of the toluene solutions of dTC-BPSAF and BPSAF at an emission maximum (λ_{em}) of 492 nm, λ_{ex} = 375 nm; inset: magnified decay curve of BPSAF. (c) The temperature-dependent transient phosphorescence decay curves of dTC-BPSAF at λ_{em} = 492 nm in toluene; λ_{ex} = 375 nm. (d) The number of TSSCs (through-space short contact with atomic distance d < 3.5 Å) of dTC-BPSAF from molecular dynamic simulation; data for BPSAF shown for comparison. (e) Kinetic traces probed at 600 nm and the corresponding fit. ΔOD, changes in absorbance. (f) The temperature effects on the average lifetimes of dTC-BPSAF and BPSAF at λ_{em} = 492 nm in toluene, λ_{ex} = 375 nm.

(25.6%; Figure S2). In contrast, for BPSAF, the T_1 state exhibits hole and electron distributions that are separately localized on the SAF donor (94.2%) and the BP acceptor (98.6%), respectively. The character of T_1 of BPSAF, which is predominantly CT (92.9%) with a small LE (7.1%) component, shifts to the hybridized local charge-transfer (HLCT) state of dTC-BPSAF, where the CT component is reduced to 56.3%, and the LE component increases to 43.7%. More importantly, the LE character of the BP acceptor (LE_A) increases significantly from 5.3% in BPSAF to 21.6% in dTC-BPSAF (Figure 2b,c). These results suggest that the acceptor dendronization can significantly enhance the LE character in the acceptor. In comparison, donor-dendronized BPSAF-DCz exhibits CT characteristics in the T_1 state with a small LE proportion of 4.67%, indicating that donor dendronization not only fails to increase the LE characteristics of BPSAF but also reduces them.

Meanwhile, the hole−electron overlap in carbonyl oxygen (overlap(O)) also displays an obvious increase after acceptor dendronization, from 5.17% in BPSAF to 12.9% in dTC-BPSAF (Figure 2b,c). Thanks to acceptor dendronization, carbonyl oxygen exhibits a large distribution degree of holes, originating from adjacent electron-donating carbazole dendritic structures. These results indicate that the acceptor dendronization strategy successfully enhances hole distributions in the acceptor and increases the $^3(n, \pi^*)$ characteristics, which can substantially increase the SOC constants and facilitate triplet radiative transitions.[37] On the contrary, the value of overlap (O) significantly decreases to as low as 0.32% in BPSAF-DCz, which is unfavorable for the n↔π transition and spin flip process. This decrease is because the donor-dendronized BPSAF-DCz enhances its electron-donating ability and weakens the hole distribution of the acceptor, leading to few $^3(n, \pi^*)$ configurations and a low likelihood of emitting RTP. Consequently, the SOC (T_1, S_0) and $\mu_{T_1 \to S_0}$ of BPSAF increase significantly from 9.07 cm^{-1} and 4.29 × 10^{-8} D to 17.35 cm^{-1} and 1.03 × 10^{-5} D for dTC-BPSAF (Figure 2d), indicating that dTC-BPSAF is expected to exhibit efficient RTP. In contrast, the SOC (T_1, S_0) is only 3.49 cm^{-1} and $\mu_{T_1 \to S_0}$ is only 1.2 × 10^{-8} D for BPSAF-DCz, suggesting that RTP is unlikely to be observed in BPSAF-DCz. These results indicate that, unlike donor dendronization, the acceptor dendronization strategy enables the dTC-BPSAF to exhibit greater LE characteristics and $^3(n, \pi^*)$ configuration, thereby facilitating RTP emission.

To explore the origin of the enhanced hole distribution in the T_1 of the acceptor in dTC-BPSAF, we statistically analyzed the contributions of HOMOs to the hole in the T_1 state of these compounds, as shown in Figure 2e and Figures S3−S6. For dTC-BPSAF, the HOMO contributes only 52.5% to the

https://doi.org/10.1021/jacs.5c06288
J. Am. Chem. Soc. 2025, 147, 18317−18326

hole of the T_1 state, with HOMO-21 and HOMO-10 accounting for 12.9 and 11.3%, respectively. In contrast, for BPSAF, HOMO contributes 95.9% while HOMO-6 contributes only 2.6% to the hole of the T_1 state. Similarly, in the donor-dendronized BPSAF-DCz, HOMO contributes 93.9%, and HOMO-4 contributes 4.6% to the hole of T_1 state. Meanwhile, the contributions of LUMO to the electron in the T_1 state of dTC-BPSAF, BPSAF, and BPSAF-DCz are significant (>80%), indicating that the effect of electron changes on the LE and LE_A properties is relatively small. These results suggest that the donor dendronization strategy fails to generate more molecular orbitals for hole distributions of the carbonyl oxygen. In comparison, the acceptor dendronization effectively modulates the electronic structure of the T_1 state, combining different mixtures of molecular orbitals to enhance the hole distributions in carbonyl oxygen and the $^3(n, \pi^*)$ configuration of the triplet state. To investigate the universality of this acceptor dendronization strategy to achieve RTP, we conducted calculations on the excited states of small molecules BPSAX and BPSAT, and the corresponding dendrimers dTC-BPSAX and dTC-BPSAT (Figures S7−S9). Our calculated findings reveal that acceptor dendronization can also lead to an increase in the ISC pathways, SOC (T_1, S_0), and $\mu_{T_1 \rightarrow S_0}$ for these dendrimers, and they are anticipated to exhibit efficient RTP. These calculated results support the universality of the acceptor dendronization strategy to achieve efficient RTP emission.

Photoluminescence Behaviors in Solution. To verify the feasibility of this acceptor dendronization strategy for achieving efficient RTP, the acceptor-dendronized dendrimer dTC-BPSAF was successfully synthesized. The synthetic routes and fundamental characterizations of dTC-BPSAF are found in Scheme S1 and Figures S10, S11, and S38−S48. The ultraviolet−visible absorption spectrum (Figure 3a) in toluene solution reveals the presence of an intramolecular charge-transfer band spanning approximately 350−400 nm and the absorption bands at 350 nm can be assigned to the $\pi-\pi^*$ transitions of the dTC-BPSAF dendrimer. In the photoluminescence (PL) spectrum measured in toluene, dTC-BPSAF exhibits a sky-blue prompt emission peak centered at 494 nm. In the delayed PL spectrum with a delayed time of 0.1 ms, dTC-BPSAF exhibits a structureless emission at 497 nm, suggesting that the long-lived emission spectra may originate from triplet states. The PL behaviors at room temperature are similar to those at a low temperature (Figure S12). The transient PL decay spectra of dTC-BPSAF and BPSAF in air-equilibrated toluene were measured for comparison (Figure 3b). dTC-BPSAF displays a significant long-lived lifetime of 1.85 ms, but BPSAF shows a noticeably shorter delayed lifetime of 161 ns. The long lifetime of dTC-BPSAF is also demonstrated in different solvents (Figure S13). To determine the origin of the much longer lifetime due to acceptor dendronization, the temperature-dependent PL decay curves of dTC-BPSAF from 198 to 378 K were measured in air (Figure 3c). The lifetimes of the long-lived components decrease monotonically with increasing temperature, which is opposite to TADF[29,30] and consistent with phosphorescence[21](Figures S14 and S15). The fluorescence and delayed fluorescence with a short lifetime of dTC-BPSAF are also observed in toluene (Figure S16). To compare the air stability, the phosphorescence decay spectrum in nitrogen-filled toluene solution of dTC-BPSAF is measured and shows a lifetime (1.92 ms) similar to that in air, indicating that the RTP from dTC-BPSAF remains highly stable in solutions with and without oxygen[38] (Figure S17). The reactive oxygen species (ROS) generation measurements[39] suggest that the triplet excitons generated by dTC-BPSAF exhibit low production of $^1O_2$, which further illustrates the high stability of dTC-BPSAF against oxygen and triplet exciton quenching (Figures S18 and S19). These results demonstrated that acceptor dendronization can efficiently suppress phosphorescence quenching caused by oxygen in solution.

The in-solution phosphorescence of dTC-BPSAF can be inferred to originate from inhibited molecular motion and suppressed nonradiative transitions. Generally, strong spatial (intermolecular and intramolecular) interactions can significantly rigidify molecular structures and limit molecular motion, which is beneficial to stable triplet exciton.[40] In dilute solutions, the distance between two solute molecules is large, and intermolecular interactions can be ignored. Therefore, intramolecular interactions of the bulky dendrons after acceptor dendronization can be attributed to the main factors affecting the molecular motion of dTC-BPSAF (Figure S20). The intramolecular interactions (atomic distance d < 3.5 Å)[41] of a single molecule can be estimated by calculating the number of through-space short contacts (TSSCs) of dTC-BPSAF based on molecular dynamics (MD) simulations using the GROMACS 2023.1 package[42] (Figure 3d). The average of TSSCs between the D-A core (red and green color) and dendrons (blue color) (Figure 1b,c) for dTC-BPSAF is 34.4, and the value of BPSAF is only 4.25 (Figure S21), indicating significantly increased intramolecular interactions due to acceptor dendronization. Therefore, the much greater intramolecular interactions of dTC-BPSAF effectively restrict molecular motion and stabilize the triplet excitons for emitting RTP in solution.

Femtosecond transient absorption measurements were conducted to probe the energy dissipation process in dTC-BPSAF and BPSAF. Upon photoexcitation at 340 nm with a pump laser, there was a rapid increase in absorption in the excited-state absorption (ESA) spectrum (Figure 3e and Figure S22), exhibiting an ESA peak at ∼600 nm. No apparent peak shift was observed in the ESA. The femtosecond transient absorption measurement of dTC-BPSAF exhibits two decay time constants, namely, 9.68 ps (derived from exciton−phonon coupling) and 631 ps (derived from energy dissipation pathway from molecular motion).[43] For BPSAF, the two decay time constants are 0.44 and 14.8 ps. The longer decay lifetime of dTC-BPSAF is attributed to the slower singlet energy dissipation pathway due to the more crowded molecular structures. The bulky molecular structure enables dTC-BPSAF to convert absorbed photons into excitons, which can slowly undergo nonradiative recombination and inefficient energy transfer from dTC-BPSAF to the surrounding solvent through molecular motion. The singlet nonradiative decay rates were calculated using the Molecular Materials Property Prediction Package (MOMAP) software.[44] The rate of acceptor-dendronized dTC-BPSAF (1.29×10^7 s^{-1}) is much smaller than that of BPSAF (3.12×10^9 s^{-1}), which is consistent with ESA dynamic results. These findings suggest that acceptor dendronization can effectively retard the energy dissipation process by restricting the structural motion.

To further explore the effects of molecular motion and PL behavior, the average PL lifetimes of dTC-BPSAF and BPSAF in toluene at different temperatures are plotted, as shown in

https://doi.org/10.1021/jacs.5c06288
J. Am. Chem. Soc. 2025, 147, 18317−18326

Figure 3f and Figure S23. In low temperatures, both exhibit phosphorescence with long lifetimes due to the highly restricted molecular motion. As the temperature increases, molecular motion becomes more vigorous, and the PL lifetime of dTC-BPSAF gradually shortens to the submillisecond level, indicating that the dendritic structure with strong intramolecular interactions can greatly suppress triplet exciton quenching at high temperatures. In contrast, the PL lifetime of BPSAF with a flexible structure sharply decreases with heating, phosphorescence rapidly disappears, and only delayed fluorescence is displayed. These results suggest that intramolecular interactions can stabilize the triplet exciton by restricting molecular motion, resulting in significantly stable phosphorescence to counterbalance the exciton loss caused by molecular thermal motion.

To directly demonstrate the molecular motion of dTC-BPSAF and BPSAF, we further employed variable temperature (VT) ^{1}H NMR in dicloromethane-d_2 to investigate their mobility (Figure 4 and Figures S24–S28). At 298 K, the ^{1}H NMR spectrum of dTC-BPSAF, with bulky dendron substituents, exhibits three species in a range of 6.0–6.8 ppm with clearly broad spectra full-widths at half-maximum (fwhm's) of 0.01 to 0.02 ppm, which are distinctively broader than those of BPSAF (0.06–0.09 ppm). This suggests that molecular rotation in dTC-BPSAF is significantly restricted at room temperature. At 223 K, the ^{1}H NMR spectrum of dTC-BPSAF in a range of 6.5–6.8 ppm clearly shows three species and condensed broad peaks at 6.1–6.3 ppm. These fwhm's of peaks of dTC-BPSAF (0.06–0.1 ppm) are significantly broader than those of BPSAF (0.01–0.02 ppm) at 223 K, indicating that acceptor dendronization more significantly suppresses molecular rotation at low temperatures.

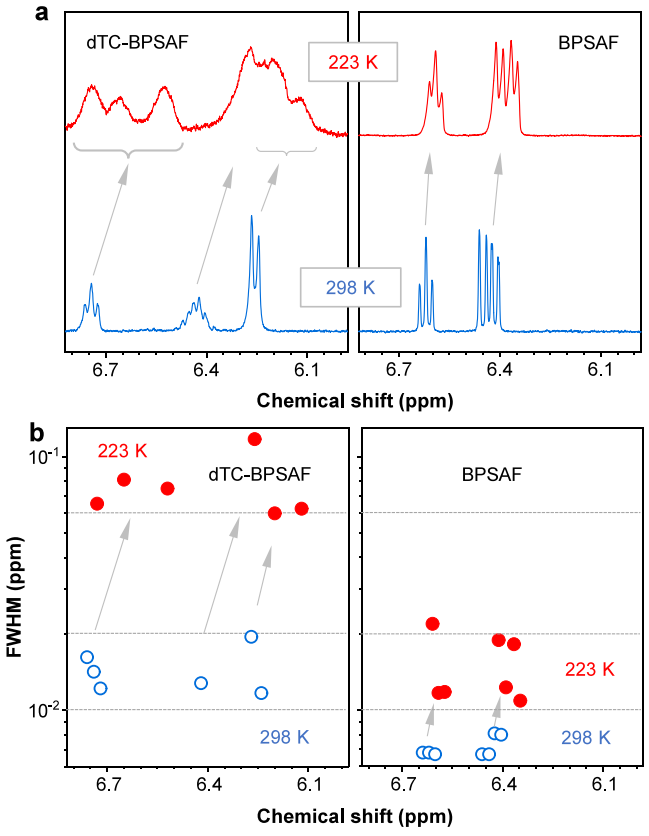

Figure 4. Molecular motions of the acceptor dendronized dendrimer dTC-BPSAF and its prototype small molecule BPSAF. (a) The broadening of ^{1}H NMR peaks with temperature; the NMR spectra of dTC-BPSAF and BPSAF were measured in CD_2Cl_2 at 223 and 298 K. (b) The decrease in the temperature leads to a broadening in the resonance peak, that is, an increase in the full width at half-maximum (fwhm).

Furthermore, upon cooling, the triplet species of dTC-BPSAF at approximately 6.7 ppm split into three peaks and undergo a significant upfield shift (Figure 4). The broad peaks at approximately 6.3 and 6.4 ppm also exhibit an upfield shift and coalesce into one species at 6.1–6.3 ppm. These upfield-shifted peaks at low temperatures are assigned to the more pronounced shielding effect of the electron cloud from nearby weak-donating dendrons due to intramolecular through-space interactions.[43] Besides, the reduction of molecular motion at low temperatures can limit the rotation and vibration of the nuclei, thereby reducing the influence of local magnetic fields on the nuclei and causing upfield-shifted peaks. In contrast, compared with dTC-BPSAF, BPSAF displays very small upfield-shifted peaks upon cooling (Figure 4), indicating a smaller reduction in molecular motion and a weaker shielding effect due to the lack of intramolecular through-space interactions. These results demonstrate that acceptor dendronization significantly restricts molecular rotation and increases intramolecular through-space interactions.

Photoluminescence Behaviors in the Aggregate State and OLED Devices. To investigate the RTP properties from solution to aggregate states, the PL properties of dTC-BPSAF in a dilute THF/water solution were measured (Figure S29 and Table S1). The PL intensity of dTC-BPSAF exhibits a significant increase with the addition of water to fractions (f_w) of 90%, indicating a pronounced aggregation-induced emission (AIE)[45] phenomenon. Concurrently, the phosphorescence lifetimes also exhibit a substantial increase from 3.2 to 28.0 ms with an increasing degree of aggregation, indicating aggregation-induced phosphorescence enhancement (AIPE)[46] behaviors. Therefore, the PLQY of dTC-BPSAF is 34% in solution and sharply increases to 63% in neat films (Figure 5a and Figure S30 and Table S2). These results indicate that restricted intramolecular motion caused by aggregation can largely block the nonradiative pathways and further improve RTP efficiency.

To fabricate the OLED devices, the PL properties of doped host films were investigated. Their prompt and delayed PL spectra of the doped host, 10-(4-((4-(9*H*-carbazol-9-yl)-phenyl)sulfonyl)phenyl)-9,9-dimethyl-9,10-dihydroacridine (CzAcSF)[47] at 10 wt % in films, exhibit PL emissions at 481 nm and phosphorescence emission at 483 nm for dTC-BPSAF, with a small ΔE_{ST} of 0.02 eV at room temperature (Figures S31 and S32 and Table S2). Moreover, the k_{ISC} of 2.07×10^7 s^{-1} for dTC-BPSAF in doped films is significantly higher than that of BPSAF (1.4×10^6 s^{-1}),[31] resulting in a high k_p of 36.0 s^{-1} for dTC-BPSAF, which indicates the successful realization of efficient RTP emission in doped films through the acceptor dendronization strategy. Consequently, the PLQY of dTC-BPSAF doped film reaches up to 98% (Figure 5a), highlighting their significant potential for the fabrication of efficient RTP-OLEDs.

In the realm of RTP-OLEDs, several significant challenges persist, hindering their advancement.[6] These obstacles include the low PLQY in amorphous films, inferior EQE of the devices, unstable electroluminescence spectra,[20] and limited molecular

https://doi.org/10.1021/jacs.5c06288
J. Am. Chem. Soc. 2025, 147, 18317–18326

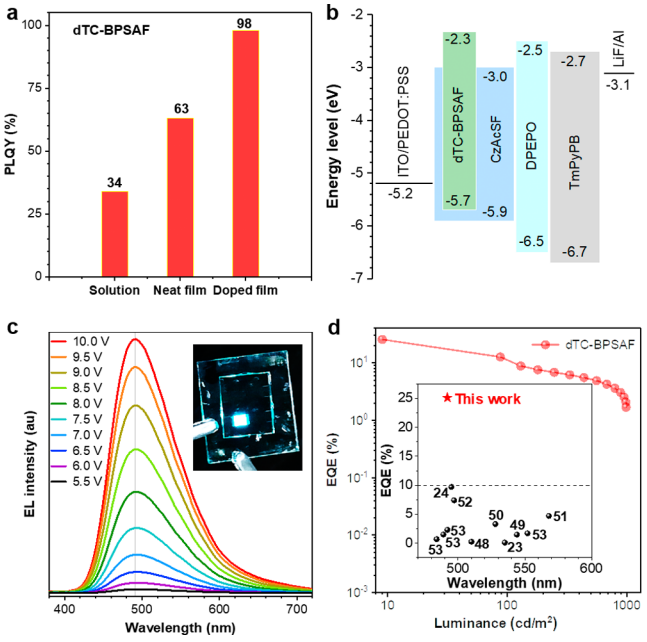

Figure 5. Device performances of the solution-processed dTC-BPSAF-based OLED devices. (a) The PLQY of dTC-BPSAF in toluene (10 μM), neat film, and doped film (CzAcSF: 10 wt % dTC-BPSAF). (b) The device configuration of the OLEDs. (c) The EL spectral stability of the OLEDs; inset: EL photo of the device measured at 6 V. (d) The EQE versus luminance plots of the OLEDs; inset: the current EQE of solution-processed RTP OLEDs versus λ_{max}^{EL}.

design strategies. These factors collectively impede the development of efficient and color-stable RTP-OLEDs. Specifically, the development of high-efficiency sky-blue RTP materials has been fundamentally constrained by the large ΔE_{ST} in conventional systems, which induces significant emission redshift and compromises sky-blue emission purity. In this work, the RTP-OLED devices were fabricated by spin-coating and vacuum evaporation with a configuration of indium tin oxide (ITO)/poly(3,4-ethylenedioxythiophene):poly(styrenesulfonate) (PEDOT:PSS) (70 nm)/10-(4-((4-(9*H*-carbazol-9-yl)phenyl)-sulfonyl)phenyl)-9,9-dimethyl-9,10-dihydroacridine (CzAcSF):dTC-BPSAF (90:10, EML, 40 nm)/bis[2-(diphenylphosphino)phenyl] ether oxide (DPEPO) (10 nm)/1,3,5-tri(m-pyrid-3-ylphenyl)benzene (TmPyPB) (50 nm)/ lithium fluoride (LiF) (1 nm)/ aluminum (Al) (100 nm) (Figure 5b). Among them, PEDOT:PSS and the emission layer were prepared by spin coating, while other layers were prepared by vacuum deposition. Detailed device data are shown in Figure 5c,d, and in Table S3. The fabricated devices exhibit sky-blue electroluminescence (EL) with a peak wavelength of 492 nm with CIE color coordinates of (0.18, 0.36). These values are slightly redshifted compared with the PL spectra in doped films. Notably, the EL spectra remained remarkably stable at different voltages, owing to the small ΔE_{ST} and near-complete overlap of fluorescence and phosphorescence spectra. This innovative acceptor dendronization strategy overcomes the critical redshift limitation in conventional sky-blue RTP-OLEDs. The devices achieve a high maximum current efficiency (CE) of 59.5 cd/A, a maximum power efficiency (PE) of 33.9 lm/W, and a maximum EQE of 25.1% (Figure S33). These results exceed the current state-of-the-art performance for any reported solution-processed RTP-OLED devices[23,24,48−53] (Figure 5d). Considering that the light out-coupling efficiency of the conventional OLEDs is 20−30%, the abovementioned devices can achieve almost a unit exciton utilization rate. In addition, Figures S34−S37 and Tables S3−S5 provide further information about devices with different structures. Among them, the solution-processed TADF-OLED based on BPSAF exhibits an EQE of 22.4%, which is worse than the performance of RTP dendrimer devices. These results indicates that the acceptor dendronization strategy can not only transfer the luminescence mechanism from TADF to RTP but also increase the device efficiency due to the reduction of nonradiative transitions. Similarly, in their nondoped device, dTC-BPSAF also shows better efficiency. Hence, the acceptor dendronization design strategy exhibits the significant potential to enhance the efficiency of RTP-OLEDs.

CONCLUSIONS

By employing our developed acceptor dendronization strategy, we have successfully achieved a series of significant advancements: (i) we have proposed a clear design rule for RTP materials at the single-molecule level and thoroughly elucidated the mechanism from facilitating ISC, boosting triplet radiation to suppressing molecular motions to achieve efficient RTP; (ii) we have developed a new type of RTP material—RTP dendrimers—and provided a theoretical basis for the development of high-performance RTP dendrimers; (iii) we have simultaneously achieved ultrastable RTP with a lifetime of 1.55 ms in ambient solution, efficient RTP films with PLQY of 98%, and state-of-art solution-processed RTP-OLEDs with an EQE_{max} of 25.1%. This breakthrough was made possible by transforming small TADF molecules into RTP dendrimers through acceptor dendronization. First, the increased splitting of triplet energy levels generates more ISC channels and enhances the ISC process. Second, introducing electron-donating dendrons into the acceptor helps to increase hole distributions within the acceptor, leading to enhanced ^3LE_A characteristics and $^3(n, \pi^*)$ transitions and significantly boosting the SOC (T_1, S_0) and $\mu_{T_1 \to S_0}$. Third, the acceptor dendronization dendrimer exhibits multiple molecular interactions that construct a rigid dendronized structure, which restricts molecular motion and stabilized triplet excitons, leading to a reduction in nonradiative transitions. Therefore, these crucial advantages, originating from acceptor dendronization, collectively lead to efficient RTP emissions in both solution and solid states, providing clear guidance for molecular design in the RTP field. Consequently, our research contributes to a deep understanding of how to regulate excited state properties and molecular motion in molecular systems to achieve efficient RTP, opening new perspectives for the development of advanced materials in the field of optoelectronics.

ASSOCIATED CONTENT

Supporting Information

The Supporting Information is available free of charge at https://pubs.acs.org/doi/10.1021/jacs.5c06288.

Synthetic pathways, structural analyses, photophysical investigations, and computational studies of the RTP dendrimer system, complemented by additional experimental details, materials, and methods, experimental

https://doi.org/10.1021/jacs.5c06288
J. Am. Chem. Soc. 2025, 147, 18317−18326

protocols, material specifications, and methodological descriptions (PDF)

AUTHOR INFORMATION

Corresponding Authors

Ben Zhong Tang − *Department of Chemistry Hong Kong Branch of Chinese National Engineering Research Center for Tissue Restoration and Reconstruction, The Hong Kong University of Science and Technology, Hong Kong 999077, China; School of Science and Engineering, Shenzhen Institute of Aggregate Science and Technology, The Chinese University of Hong Kong, Shenzhen (CUHK-Shenzhen), Shenzhen, Guangdong 518172, China;* orcid.org/0000-0002-0293-964X; Email: zhaozheng@cuhk.edu.cn

Zhongjie Ren − *State Key Laboratory of Chemical Resource Engineering, College of Materials Science and Engineering, Beijing University of Chemical Technology, Beijing 100029, China;* orcid.org/0000-0002-7981-4431; Email: lrhu@chem.ecnu.edu.cn

Guohua Xie − *The Institute of Flexible Electronics (Future Technologies), Xiamen University, Xiamen 361005, China;* orcid.org/0000-0003-0764-7889; Email: ifeghxie@xmu.edu.cn

Lianrui Hu − *Shanghai Key Laboratory of Green Chemistry and Chemical Processes, Shanghai Frontiers Science Center of Molecule Intelligent Syntheses, School of Chemistry and Molecular Engineering, East China Normal University, Shanghai 200062, China*; Email: renzj@mail.buct.edu.cn

Zheng Zhao − *School of Science and Engineering, Shenzhen Institute of Aggregate Science and Technology, The Chinese University of Hong Kong, Shenzhen (CUHK-Shenzhen), Shenzhen, Guangdong 518172, China;* orcid.org/0000-0002-5536-0439; Email: tangbenz@cuhk.edu.cn

Authors

Chensen Li − *Department of Chemistry Hong Kong Branch of Chinese National Engineering Research Center for Tissue Restoration and Reconstruction, The Hong Kong University of Science and Technology, Hong Kong 999077, China; Key Laboratory for Soft Chemistry and Functional Materials of Ministry of Education, School of Chemistry and Chemical Engineering, Nanjing University of Science and Technology, Nanjing, Jiangsu 210094, China*

Zhenchen Lou − *Shanghai Key Laboratory of Green Chemistry and Chemical Processes, Shanghai Frontiers Science Center of Molecule Intelligent Syntheses, School of Chemistry and Molecular Engineering, East China Normal University, Shanghai 200062, China*

Minghui Wu − *Joint International Research Laboratory of Animal Health and Food Safety of Ministry of Education and Single Molecule Nanobiology Laboratory (Sinmolab), Nanjing Agricultural University, Nanjing, Jiangsu 210095, China*

Fulong Ma − *School of Science and Engineering, Shenzhen Institute of Aggregate Science and Technology, The Chinese University of Hong Kong, Shenzhen (CUHK-Shenzhen), Shenzhen, Guangdong 518172, China*

Xinmeng Chen − *Department of Chemistry Hong Kong Branch of Chinese National Engineering Research Center for Tissue Restoration and Reconstruction, The Hong Kong University of Science and Technology, Hong Kong 999077, China*

Haozhe Tan − *School of Science and Engineering, Shenzhen Institute of Aggregate Science and Technology, The Chinese University of Hong Kong, Shenzhen (CUHK-Shenzhen), Shenzhen, Guangdong 518172, China*

Zonghang Liu − *School of Science and Engineering, Shenzhen Institute of Aggregate Science and Technology, The Chinese University of Hong Kong, Shenzhen (CUHK-Shenzhen), Shenzhen, Guangdong 518172, China*

Feng Gao − *School of Science and Engineering, Shenzhen Institute of Aggregate Science and Technology, The Chinese University of Hong Kong, Shenzhen (CUHK-Shenzhen), Shenzhen, Guangdong 518172, China*

Zijie Qiu − *School of Science and Engineering, Shenzhen Institute of Aggregate Science and Technology, The Chinese University of Hong Kong, Shenzhen (CUHK-Shenzhen), Shenzhen, Guangdong 518172, China;* orcid.org/0000-0003-0728-1178

Maoqiu Li − *State Key Laboratory of Chemical Resource Engineering, College of Materials Science and Engineering, Beijing University of Chemical Technology, Beijing 100029, China*

Yumeng Guo − *State Key Laboratory of Chemical Resource Engineering, College of Materials Science and Engineering, Beijing University of Chemical Technology, Beijing 100029, China*

Song Zhang − *State Key Laboratory of Magnetic Resonance and Atomic and Molecular Physics, Innovation Academy for Precision Measurement Science and Technology, Chinese Academy of Sciences, Wuhan 430071, China;* orcid.org/0000-0001-9816-4094

Yuchao Liu − *Key Laboratory of Rubber-Plastics, Ministry of Education, Qingdao University of Science and Technology, Qingdao 266042, China;* orcid.org/0000-0001-9088-3852

Shouke Yan − *State Key Laboratory of Chemical Resource Engineering, College of Materials Science and Engineering, Beijing University of Chemical Technology, Beijing 100029, China; Key Laboratory of Rubber-Plastics, Ministry of Education, Qingdao University of Science and Technology, Qingdao 266042, China;* orcid.org/0000-0003-1627-341X

Zhen Li − *Hubei Key Lab on Organic and Polymeric Optoelectronic Materials, Tai Kang Center for Life and Medical Sciences, Sauvage Center for Molecular Sciences, Department of Chemistry, Wuhan University, Wuhan 430072, China;* orcid.org/0000-0002-1512-1345

Bo Xu − *Key Laboratory for Soft Chemistry and Functional Materials of Ministry of Education, School of Chemistry and Chemical Engineering, Nanjing University of Science and Technology, Nanjing, Jiangsu 210094, China;* orcid.org/0000-0002-4703-7340

Ryan T. K. Kwok − *Department of Chemistry Hong Kong Branch of Chinese National Engineering Research Center for Tissue Restoration and Reconstruction, The Hong Kong University of Science and Technology, Hong Kong 999077, China;* orcid.org/0000-0002-6866-3877

Jacky W. Y. Lam − *Department of Chemistry Hong Kong Branch of Chinese National Engineering Research Center for Tissue Restoration and Reconstruction, The Hong Kong University of Science and Technology, Hong Kong 999077, China*

Complete contact information is available at:

https://doi.org/10.1021/jacs.5c06288
J. Am. Chem. Soc. 2025, 147, 18317−18326

https://pubs.acs.org/10.1021/jacs.5c06288

Author Contributions

‡C.L., Z. Lou, M.W., and F.M. contributed equally. All authors have given approval to the final version of the manuscript.

Notes

The authors declare no competing financial interest.

■ ACKNOWLEDGMENTS

This work was supported by the National Natural Science Foundation of China Grant (52273197, 52333007, 22103062, 52373195, 52273164, 12274418, and 22304071); the Research Grants Council of Hong Kong (16304819, 16305320, and C6014-20W); the Innovation and Technology Commission (ITCCNERC14SC01); the Shenzhen Key Laboratory of Functional Aggregate Materials (ZDSYS 20211021111400001); the Science, Technology and Innovation Commission of Shenzhen Municipality (GJHZ 20210705141810031, JCYJ 2021324134613038, KQTD 20210811090142053, GJHZ 20210705141810031); Shanghai Pujiang Program (no. 22PJ1402800); Shandong Provincial Natural Science Foundation (ZR2022ZD37); the Fundamental Research Funds for the Central Universities (QNTD20). The authors thank to the AIE Institute (www.aietech.org.cn) for providing some technical assistance and the Materials Characterization and Preparation Center, The Chinese University of Hong Kong, Shenzhen, for material characterization.

■ REFERENCES

(1) Bolton, O.; Lee, K.; Kim, H. J.; Lin, K. Y.; Kim, J. Activating efficient phosphorescence from purely organic materials by crystal design. *Nat. Chem.* **2011**, *3*, 205−210.

(2) An, Z.; Zheng, C.; Tao, Y.; Chen, R.; Shi, H.; Chen, T.; Wang, Z.; Li, H.; Deng, R.; Liu, X.; Huang, W. Stabilizing triplet excited states for ultralong organic phosphorescence. *Nat. Mater.* **2015**, *14*, 685−690.

(3) Gu, L.; Shi, H.; Bian, L.; Gu, M.; Ling, K.; Wang, X.; Ma, H.; Cai, S.; Ning, W.; Fu, L.; Wang, H.; Wang, S.; Gao, Y.; Yao, W.; Huo, F.; Tao, Y.; An, Z.; Liu, X.; Huang, W. Colour-tunable ultra-long organic phosphorescence of a single-component molecular crystal. *Nat. Photonics* **2019**, *13*, 406−411.

(4) Zhao, W.; He, Z.; Tang, B. Z. Room-temperature phosphorescence from organic aggregates. *Nat. Rev. Mater.* **2020**, *5*, 869−885.

(5) Ye, W.; Ma, H.; Shi, H.; Wang, H.; Lv, A.; Bian, L.; Zhang, M.; Ma, C.; Ling, K.; Gu, M.; Mao, Y.; Yao, X.; Gao, C.; Shen, K.; Jia, W.; Zhi, J.; Cai, S.; Song, Z.; Li, J.; Zhang, Y.; Lu, S.; Liu, K.; Dong, C.; Wang, Q.; Zhou, Y.; Yao, W.; Zhang, Y.; Zhang, H.; Zhang, Z.; Hang, X.; An, Z.; Liu, X.; Huang, W. Confining isolated chromophores for highly efficient blue phosphorescence. *Nat. Mater.* **2021**, *20*, 1539−1544.

(6) Zhou, Z.; Xie, X.; Sun, Z.; Wang, X.; An, Z.; Huang, W. Recent advances in metal-free phosphorescent materials for organic light-emitting diodes. *J. Mater. Chem. C* **2023**, *11*, 3143−3161.

(7) Wang, D.; Gong, J.; Xiong, Y.; Wu, H.; Zhao, Z.; Wang, D.; Tang, B. Z. Achieving Color-Tunable and Time-Dependent Organic Long Persistent Luminescence via Phosphorescence Energy Transfer for Advanced Anti-Counterfeiting. *Adv. Funct. Mater.* **2023**, *33*, 2208895.

(8) Zhang, Y.; Li, H.; Yang, M.; Dai, W.; Shi, J.; Tong, B.; Cai, Z.; Wang, Z.; Dong, Y.; Yu, X. Organic room-temperature phosphorescence materials for bioimaging. *Chem. Commun.* **2023**, *59*, 5329−5342.

(9) Zhen, X.; Qu, R.; Chen, W.; Wu, W.; Jiang, X. The development of phosphorescent probes for in vitro and in vivo bioimaging. *Biomater. Sci.* **2021**, *9*, 285−300.

(10) DeRosa, C. A.; Seaman, S. A.; Mathew, A. S.; Gorick, C. M.; Fan, Z.; Demas, J. N.; Peirce, S. M.; Fraser, C. L. Oxygen Sensing Difluoroboron beta-Diketonate Polylactide Materials with Tunable Dynamic Ranges for Wound Imaging. *ACS Sens.* **2016**, *1*, 1366−1373.

(11) Matsuoka, H.; Retegan, M.; Schmitt, L.; Höger, S.; Neese, F.; Schiemann, O. Time-resolved electron paramagnetic resonance and theoretical investigations of metal-free room-temperature triplet emitters. *J. Am. Chem. Soc.* **2017**, *139*, 12968−12975.

(12) Yuan, W. Z.; Shen, X. Y.; Zhao, H.; Lam, J. W.; Tang, L.; Lu, P.; Wang, C.; Liu, Y.; Wang, Z.; Zheng, Q. Crystallization-induced phosphorescence of pure organic luminogens at room temperature. *J. Phys. Chem. C* **2010**, *114*, 6090−6099.

(13) Yang, J.; Zhen, X.; Wang, B.; Gao, X.; Ren, Z.; Wang, J.; Xie, Y.; Li, J.; Peng, Q.; Pu, K.; Li, Z. The influence of the molecular packing on the room temperature phosphorescence of purely organic luminogens. *Nat. Commun.* **2018**, *9*, 840.

(14) Yan, Z. A.; Lin, X.; Sun, S.; Ma, X.; Tian, H. Activating Room-Temperature Phosphorescence of Organic Luminophores via External Heavy-Atom Effect and Rigidity of Ionic Polymer Matrix. *Angew. Chem., Int. Ed.* **2021**, *60*, 19735−19739.

(15) Hamzehpoor, E.; Ruchlin, C.; Tao, Y.; Liu, C. H.; Titi, H. M.; Perepichka, D. F. Efficient room-temperature phosphorescence of covalent organic frameworks through covalent halogen doping. *Nat. Chem.* **2023**, *15*, 83−90.

(16) Ma, X.; Wang, J.; Tian, H. Assembling-Induced Emission: An Efficient Approach for Amorphous Metal-Free Organic Emitting Materials with Room-Temperature Phosphorescence. *Acc. Chem. Res.* **2019**, *52*, 738−748.

(17) Ma, X. K.; Liu, Y. Supramolecular Purely Organic Room-Temperature Phosphorescence. *Acc. Chem. Res.* **2021**, *54*, 3403−3414.

(18) Li, W.; Huang, Q.; Mao, Z.; Zhao, J.; Wu, H.; Chen, J.; Yang, Z.; Li, Y.; Yang, Z.; Zhang, Y.; Aldred, M. P.; Chi, Z. Selective expression of chromophores in a single molecule: soft organic crystals exhibiting full-colour tunability and dynamic triplet-exciton behaviours. *Angew. Chem., Int. Ed.* **2020**, *59*, 3739−3745.

(19) Zhang, T.; Ma, X.; Wu, H.; Zhu, L.; Zhao, Y.; Tian, H. Molecular engineering for metal-free amorphous materials with room-temperature phosphorescence. *Angew. Chem., Int. Ed.* **2020**, *59*, 11206−11216.

(20) Chen, Z.; Li, M.; Gu, Q.; Peng, X.; Qiu, W.; Xie, W.; Liu, D.; Jiao, Y.; Liu, K.; Zhou, J.; Su, S. J. Highly efficient purely organic phosphorescence light-emitting diodes employing a donor-acceptor skeleton with a phenoxaselenine donor. *Adv. Sci.* **2023**, *10*, No. e2207003.

(21) Peng, X.; Zou, P.; Zeng, J.; Wu, X.; Xie, D.; Fu, Y.; Yang, D.; Ma, D.; Tang, B. Z.; Zhao, Z. Purely Organic Room-Temperature Phosphorescence Molecule for High-Performance Non-Doped Organic Light-Emitting Diodes. *Angew. Chem., Int. Ed.* **2024**, *63*, No. e202405418.

(22) Zou, Y.; Gong, S.; Xie, G.; Yang, C. Design Strategy for Solution-Processable Thermally Activated Delayed Fluorescence Emitters and Their Applications in Organic Light-Emitting Diodes. *Adv. Opt. Mater.* **2018**, *6*, 1800568.

(23) Bergamini, G.; Fermi, A.; Botta, C.; Giovanella, U.; Di Motta, S.; Negri, F.; Peresutti, R.; Gingras, M.; Ceroni, P. A persulfurated benzene molecule exhibits outstanding phosphorescence in rigid environments: from computational study to organic nanocrystals and OLED applications. *J. Mater. Chem. C* **2013**, *1*, 2717.

(24) Liu, X.; Yang, L.; Li, X.; Zhao, L.; Wang, S.; Lu, Z. H.; Ding, J.; Wang, L. An Electroactive Pure Organic Room-Temperature Phosphorescence Polymer Based on a Donor-Oxygen-Acceptor Geometry. *Angew. Chem., Int. Ed.* **2021**, *60*, 2455−2463.

(25) Tomalia, D. A.; Baker, H.; Dewald, J.; Hall, M.; Kallos, G.; Martin, S.; Roeck, J.; Ryder, J.; Smith, P. J. P. j. A New Class of Polymers: Starburst-Dendritic Macromolecules. *Polym. J.* **1985**, *17*, 117−132.

(26) Li, C.; Harrison, A. K.; Liu, Y.; Zhao, Z.; Zeng, C.; Dias, F. B.; Ren, Z.; Yan, S.; Bryce, M. R. Asymmetrical-Dendronized TADF Emitters for Efficient Non-doped Solution-Processed OLEDs by

Eliminating Degenerate Excited States and Creating Solely Thermal Equilibrium Routes. *Angew. Chem., Int. Ed.* **2022**, *61*, No. e202115140.
(27) Li, C.; Harrison, A. K.; Liu, Y.; Zhao, Z.; Dias, F. B.; Zeng, C.; Yan, S.; Bryce, M. R.; Ren, Z. TADF Dendronized Polymer with Vibrationally Enhanced Direct Spin-Flip between Charge-Transfer States for Efficient Non-doped Solution-Processed OLEDs. *Chem. Eng. J.* **2022**, *435*, No. 134924.
(28) Liu, D.; Zhang, M.; Tian, W.; Jiang, W.; Sun, Y.; Zhao, Z.; Tang, B. Z. Molecular core−shell structure design: Facilitating delayed fluorescence in aggregates toward highly efficient solution-processed OLEDs. *Aggregate* **2022**, *3*, No. e164.
(29) Uoyama, H.; Goushi, K.; Shizu, K.; Nomura, H.; Adachi, C. Highly efficient organic light-emitting diodes from delayed fluorescence. *Nature* **2012**, *492*, 234−238.
(30) Liu, Y.; Li, C.; Ren, Z.; Yan, S.; Bryce, M. R. All-organic thermally activated delayed fluorescence materials for organic light-emitting diodes. *Nat. Rev. Mater.* **2018**, *3*, 18020.
(31) Fu, Y.; Liu, H.; Yang, D.; Ma, D.; Zhao, Z.; Tang, B. Z. Boosting external quantum efficiency to 38.6% of sky-blue delayed fluorescence molecules by optimizing horizontal dipole orientation. *Sci. Adv.* **2021**, *7*, No. eabj2504.
(32) Li, A.; Tang, S.; Tan, P.; Liu, C.; Liang, B. Measurement and Prediction of Oxygen Solubility in Toluene at Temperatures from 298.45 to 393.15 K and Pressures up to 1.0 MPa. *J. Chem. Eng. Data* **2007**, *52*, 2339−2344.
(33) Ma, H.; Peng, Q.; An, Z.; Huang, W.; Shuai, Z. Efficient and Long-Lived Room-Temperature Organic Phosphorescence: Theoretical Descriptors for Molecular Designs. *J. Am. Chem. Soc.* **2019**, *141*, 1010−1015.
(34) Hirata, S. Recent Advances in Materials with Room-Temperature Phosphorescence: Photophysics for Triplet Exciton Stabilization. *Adv. Opt. Mater.* **2017**, *5*, 1700116.
(35) Lu, T.; Chen, F. Multiwfn: a multifunctional wavefunction analyzer. *J. Comput. Chem.* **2012**, *33*, 580−592.
(36) Liu, Z.; Lu, T.; Chen, Q. An sp-hybridized all-carboatomic ring, cyclo[18]carbon: Electronic structure, electronic spectrum, and optical nonlinearity. *Carbon* **2020**, *165*, 461−467.
(37) Shi, Y.; Ma, H.; Sun, Z.; Zhao, W.; Sun, G.; Peng, Q. Optimal Dihedral Angle in Twisted Donor-Acceptor Organic Emitters for Maximized Thermally Activated Delayed Fluorescence. *Angew. Chem., Int. Ed.* **2022**, *61*, No. e202213463.
(38) Wilkinson, F.; Abdel-Shafi, A. A. Mechanism of Quenching of Triplet States by Oxygen: Biphenyl Derivatives in Acetonitrile. *J. Phys. Chem. A* **1997**, *101*, 5509−5516.
(39) Liu, S.; Wang, B.; Yu, Y.; Liu, Y.; Zhuang, Z.; Zhao, Z.; Feng, G.; Qin, A.; Tang, B. Z. Cationization-Enhanced Type I and Type II ROS Generation for Photodynamic Treatment of Drug-Resistant Bacteria. *ACS Nano* **2022**, *16*, 9130−9141.
(40) Cai, S.; Yao, X.; Ma, H.; Shi, H.; An, Z. Manipulating intermolecular interactions for ultralong organic phosphorescence. *Aggregate* **2023**, *4*, No. e320.
(41) Taylor, R. Which intermolecular interactions have a significant influence on crystal packing? *CrystEngComm* **2014**, *16*, 6852−6865.
(42) Abraham, M. J.; Murtola, T.; Schulz, R.; Páll, S.; Smith, J. C.; Hess, B.; Lindahl, E. GROMACS: High performance molecular simulations through multi-level parallelism from laptops to supercomputers. *SoftwareX* **2015**, *1*, 19−25.
(43) Chen, J.; Gu, P.; Ran, G.; Zhang, Y.; Li, M.; Chen, B.; Lu, H.; Han, Y. Z.; Zhang, W.; Tang, Z.; Yan, Q.; Sun, R.; Fu, X.; Chen, G.; Shi, Z.; Wang, S.; Liu, X.; Li, J.; Wang, L.; Zhu, Y.; Shen, J.; Tang, B. Z.; Fan, C. Atomically precise photothermal nanomachines. *Nat. Mater.* **2024**, *23*, 271−280.
(44) Niu, Y.; Li, W.; Peng, Q.; Geng, H.; Yi, Y.; Wang, L.; Nan, G.; Wang, D.; Shuai, Z. MOlecular MAterials Property Prediction Package (MOMAP) 1.0: a software package for predicting the luminescent properties and mobility of organic functional materials. *Mol. Phys.* **2018**, *116*, 1078−1090.
(45) Zhao, Z.; Zhang, H.; Lam, J. W. Y.; Tang, B. Z. Aggregation-Induced Emission: New Vistas at the Aggregate Level. *Angew. Chem., Int. Ed.* **2020**, *59*, 9888−9907.
(46) Sathish, V.; Ramdass, A.; Thanasekaran, P.; Lu, K.-L.; Rajagopal, S. Aggregation-induced phosphorescence enhancement (AIPE) based on transition metal complexes—An overview. *J. Photochem. Photobiol., C* **2015**, *23*, 25−44.
(47) Lee, D. R.; Kim, M.; Jeon, S. K.; Hwang, S. H.; Lee, C. W.; Lee, J. Y. Design strategy for 25% external quantum efficiency in green and blue thermally activated delayed fluorescent devices. *Adv. Mater.* **2015**, *27*, 5861−5867.
(48) Anzenbacher, P.; Pérez-Bolívar, C.; Takizawa, S.-y.; Brega, V. Room-temperature electrophosphorescence from an all-organic material. *J. Lumin.* **2016**, *180*, 111−116.
(49) Xie, G.; Wang, J.; Xue, X.; Li, H.; Guo, N.; Li, H.; Wang, D.; Li, M.; Huang, W.; Chen, R.; Tao, Y. Achieving low driving voltage and high-efficiency afterglow organic light-emitting diodes through host−guest doping. *Appl. Phys. Rev.* **2022**, *9*, No. 031410.
(50) Si, C.; Wang, T.; Gupta, A. K.; Cordes, D. B.; Slawin, A. M. Z.; Siegel, J. S.; Zysman-Colman, E. Room-Temperature Multiple Phosphorescence from Functionalized Corannulenes: Temperature Sensing and Afterglow Organic Light-Emitting Diode. *Angew. Chem., Int. Ed.* **2023**, *62*, No. e202309718.
(51) Acharya, N.; Hasan, M.; Dey, S.; Lo, S.-C.; Namdas, E. B.; Ray, D. Phenothiazine-Quinoline Conjugates Realizing Intrinsic Thermally Activated Delayed Fluorescence and Room-Temperature Phosphorescence: Understanding the Mechanism and Electroluminescence Devices. *Adv. Photonics Res.* **2021**, *2*, 2000201.
(52) Tian, Y.; He, R.; Meng, G.; Wang, S.; Zhao, L.; Ding, J. Solution-processed orange and white OLEDs sensitized by an electroactive pure organic room-temperature phosphorescent polymer. *Mater. Adv.* **2023**, *4*, 3323−3329.
(53) Silva, W. d. P.; Decarli, N. O.; Espíndola, L.; Erfurt, K.; Blacha-Grzechnik, A.; Pander, P.; Lapkowski, M.; Data, P. Multifunctional properties of D−A luminophores based on acenaphtopyrido[2,3-b]pyrazine core: photophysics, photochemistry, and efficient solution-processed OLEDs. *J. Mater. Chem. C* **2023**, *11*, 15246−15260.

https://doi.org/10.1021/jacs.5c06288
J. Am. Chem. Soc. 2025, 147, 18317−18326